DESY 14-077
LPN 14-076
SFB/CPP-14-27

Top-quark pair production at hadron colliders: differential cross section and phenomenological applications with DiffTop

Marco Guzzi[a], Katerina Lipka[a] and Sven-Olaf Moch[b,c]

[a] *Deutsches Elektronen-Synchrotron DESY,*
Notkestrasse 85, D-22607 Hamburg, Germany

[b] *II. Institut für Theoretische Physik, Universität Hamburg,*
Luruper Chaussee 149, D-22761 Hamburg, Germany

[c] *Deutsches Elektronen-Synchrotron DESY,*
Platanenallee 6, D-15738 Zeuthen, Germany [1]

Abstract

The results of phenomenological studies of top-quark pair production in proton-proton collisions are presented. Differential cross sections are calculated in perturbative QCD at approximate next-to-next-to-leading order $\mathcal{O}(\alpha_s^4)$ by using methods of threshold resummation beyond the leading logarithmic accuracy. Predictions for the single-particle inclusive kinematics are presented for transverse momentum and rapidity distributions of final-state top quarks. Uncertainties related to the description of proton structure, top-quark mass and strong coupling constant are investigated in detail. The results are compared to the recent measurements by the ATLAS and CMS collaborations at the LHC at the center of mass energy of 7 TeV. The calculation presented here is implemented in the computer code DIFFTOP and can be applied to the general case of heavy-quark pair production at hadron-hadron colliders.

[1] marco.guzzi@desy.de, katerina.lipka@desy.de, sven-olaf.moch@desy.de

1 Introduction

Studies of heavy-quark production at hadron colliders provide stringent tests of quantum chromodynamics (QCD) and of the theory of electroweak (EW) interactions. Furthermore, these are of crucial importance in searches for signatures of physics Beyond the Standard Model (BSM). The mass of the recently discovered Higgs boson [1, 2] has been measured to be in the range $120 \leq m_H \leq 135$ GeV, therefore the Higgs sector is expected to be closely related to the physics of the top-quark. In particular, the role of quantum corrections to the top-quark mass, which together with the mass of the Higgs-boson define the electroweak vacuum stability conditions has been studied [3, 4].

Experimentally, top-quark physics is being studied at the Tevatron and is extensively explored at the unprecedented energies of the Large Hadron Collider (LHC). The CMS, ATLAS, DØ, and CDF collaborations have recently combined their results [5] for the top-quark mass and obtained a value of $m_t = 173.3 \pm 0.76$ GeV. The interpretation of the measured mass and its relation to the theoretically well-defined pole mass of the top quark is discussed in details in [6]. New observables to be used for the measurement of the top-quark mass at hadron colliders are proposed in [7,8]. The most recent determination of the pole mass of the top quark is performed by the CMS collaboration [9]. In the same analysis, for the first time, the issue of correlations between the top-quark pole mass, gluon distribution, and strong coupling constant α_s in QCD predictions for the inclusive cross section of top-quark pair production is discussed.

Precise measurements for the total and differential cross section for top-quark pair production at a center-of-mass energies $\sqrt{S} = 7$ and 8 TeV have been recently published by the CMS [10,11] and ATLAS [12–14] collaborations. The interpretation of current and forthcoming LHC data demands high-precision theory predictions that imply a new realm of precision calculations in perturbative QCD (pQCD), supplied by the development of efficient tools for phenomenological analyses. The QCD corrections to heavy-quark production at hadron colliders at the next-to-leading order (NLO), $\mathcal{O}(\alpha_s^3)$, are known since many years [15–20]. The full calculation at next-to-next-to-leading order (NNLO), $\mathcal{O}(\alpha_s^4)$, for the inclusive cross section has been accomplished only recently [21–24] and required continuous efforts of the QCD community in calculating radiative corrections and in the development of computational tools [25–32]. The NNLO calculation of the inclusive cross section for the $t\bar{t}$ production is implemented in the C++ computer programs Top++ [21] and Hathor [33]. In these calculations the final-state top quarks are considered in the on-shell approximation. Studies in QCD at NLO where final-state top quarks decay into pairs of W bosons and b quarks can be found in Ref. [34–36].

The comparison of QCD predictions with the data and a multitude of phenomenological analyses of interest require to have precise predictions not only for the inclusive cross section, but also at differential level. Invariant mass distribution of $t\bar{t}$, transverse momentum and rapidity distributions of the top quark or $t\bar{t}$, are examples of differential distributions needed at the

highest perturbative order possible. The exact NLO calculations for $t\bar{t}$ total and differential cross sections are implemented into Monte Carlo (MC) numerical codes MCFM [37], MC@NLO [38], POWHEG [39], MadGraph/MadEvent [40,41]. The NNLO corrections for these observables are not yet available.

In this paper, we present the approximate NNLO $\mathcal{O}(\alpha_s^4)$ calculation for the differential cross section in the single-particle inclusive (1PI) kinematic for heavy-flavor production at hadron colliders. Techniques of logarithmic expansion beyond the leading logarithmic accuracy in QCD threshold resummation are used. This calculation is implemented in a novel computer code DiffTop. In this paper, phenomenological studies with DiffTop are presented, that are of importance for future analyses at the LHC.

1.1 Prospects for determination of the gluon distribution using $t\bar{t}$ production

Top-pair production at the LHC probes parton distribution functions (PDFs) of the proton, in particular the gluon distribution. In proton-proton collisions at the LHC, $t\bar{t}$ production is mainly driven by the gluon, in fact approximately 85% of the total cross section is ascribed to the gluon-gluon channel at $\sqrt{S} = 7$ TeV and this fraction grows with the increase of $\sqrt{S}$. Measurements of the $t\bar{t}$ total and differential cross sections offer the possibility of probing the gluon in the large Bjorken x region ($x \approx 0.1$) where gluon is currently poorly constrained. This has first been studied in [42] (see also [43]). However, strong correlations between α_s, gluon distribution $g(x)$, and the pole mass of the top quark m_t, in the QCD description of $t\bar{t}$ production have to be taken into account. A simultaneous determination of $g(x)$, α_s and m_t, using the $t\bar{t}$ measurements at the LHC in a QCD analysis, together with measurements of Deep-Inelastic Scattering (DIS) and jet production in DIS and proton-proton collisions might resolve these correlations.

The developments presented in this paper provide a basis for the inclusion of differential $t\bar{t}$ cross sections into QCD analyses at approximate NNLO. For the purpose of a fast calculation within QCD analyses for PDF determination, DiffTop is being interfaced to fastNLO [44–47] which allows the user to calculate fast theory predictions using any PDFs. This represents a clear advantage in terms of the CPU-time consumption.

1.2 Threshold resummation techniques

The new LHC measurements give us the possibility of investigating the applicability of QCD factorization for hadronic cross sections with high precision. In the past three decades QCD techniques have experienced stages of remarkable progress on theoretical and phenomenological ground. In particular, theoretical tools were introduced to estimate the importance of the perturbative higher orders in cross-section calculations [48–53]. In Fig. 1 we show the top-quark transverse momentum, p_T^t, where higher orders are important and have reduced scale dependence.

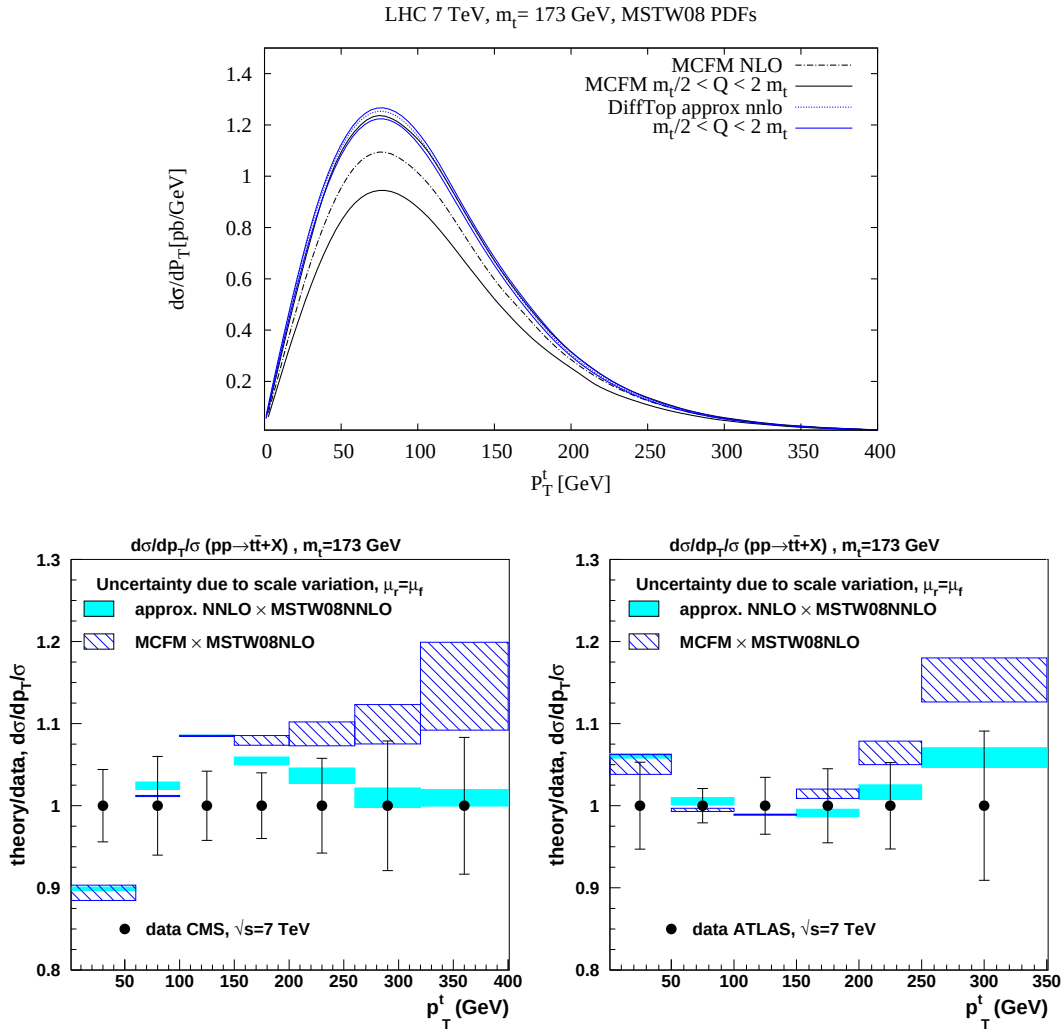

Figure 1: Study of scale uncertainties for MCFM and DiffTop calculations for the top-quark p_T^t distribution. Upper inset: absolute p_T^t distribution at NLO with MCFM (hatched band), and approx. NNLO with DiffTop (shaded band). Lower inset: ratio of theory over data for CMS (left) [10] and ATLAS (right) [12] measurements. Here MSTW08 NLO (NNLO) PDFs are used for the MCFM (DiffTop) calculation. Renormalization and factorization scales are set to $\mu_R = \mu_F = m_t$ and varied such as $m_t/2 \leq \mu_R = \mu_F \leq 2m_t$.

The non-unique separation between long- and short-distance dynamics of partons in the proton is understood in terms of factorization theorems, in which inclusive hadronic cross sections are factorized in universal nonperturbative PDFs and fragmentation functions (FF), and hard scattering coefficients that can be computed in perturbative QCD. These hard scattering functions still contain, in certain kinematic regions, residuals of long-distance dynamic related to leftovers in the cancellation between real and virtual soft-gluon contributions. These finite reminders limit the predictive power of QCD in the kinematic region close to the partonic production threshold where singular logarithmic terms give large corrections to the cross section. Threshold resummation methods, which are based on the universality of soft-gluon cancellation, allow us to resum these large contributions to all orders so that the predictive power of pQCD is extended to the phase space regions of the partonic threshold. By using threshold resummation methods one can derive approximate formulas at NNLO for differential distributions, in which the cross sections are expanded in terms of the logarithmic enhanced contributions (appearing as plus distributions), and can therefore be written at various degrees of logarithmic accuracy. Studies at the next-to-leading-logarithmic (NLL), next-to-next-to-leading-logarithmic (NNLL) accuracy and beyond can be found in Refs. [54–62] and references therein.

Recently, methods of heavy-quark effective theory (HQET) and soft-collinear effective theory (SCET) experienced enormous progress and received significant attention. Such methods can be also used to write the factorization formula for the hard-scattering kernels in the threshold region [63–66]. Approximate NNLO calculations, based on SCET, for differential cross sections for heavy-quark production can be found in [67–73] and references therein. A study of differences and similarities between the traditional QCD threshold resummation formalism and SCET can be found in [74] for the $t\bar{t}$ case.

2 Single particle kinematic

Top-quark pairs are produced in hadronic reactions in which the scattering process is defined by

$$H_1(P_1) + H_2(P_2) \to t(p_1) + \bar{t}(p_2) + X(k)\,, \tag{1}$$

where H_1 and H_2 are the incoming hadrons with momenta P_1 and P_2 respectively, the final state top-quark has momentum p_1, the anti-top mometum p_2 and $X(k)$ represents any inclusive hadronic final state allowed by the reaction. At phenomenological level, the differential cross sections of interest are written in such a way that can be compared to measurements that are related to the detection of single particles or particle pairs.

When a single particle is detected in the final state, for instance the top-quark, the one-particle inclusive (1PI) kinematic is used to determine the p_T^t spectrum and the rapidity y^t distribution of the top-quark. These distributions are obtained by integrating over the phase space of the anti-top (not observed) together with any real emission of radiation [52].

When particle pairs are detected, the pair-invariant mass kinematic (PIM) is used to write a factorized cross section [48, 49, 51, 53, 75] in terms of the invariant mass of the heavy system, collective rapidity, and additional variables like the angle between the final-state quark direction and the beam axis. In what follows we will discuss differential distributions derived in the 1PI kinematic case and will leave the PIM kinematic [55] for a forthcoming analysis[2].

In the case of single particle detection, the reaction in Eq.(1) is written as

$$H_1(P_1) + H_2(P_2) \to t(p_1) + X[\bar{t}](p_2')\,, \tag{2}$$

where p_2' represents the recoil momentum. The Mandelstam invariants at hadronic level are defined as

$$S = (P_1+P_2)^2\,,\quad T_1 = (P_2-p_1)^2 - m_t^2\,,\quad U_1 = (P_1-p_1)^2 - m_t^2\,,\quad S_4 = S+T_1+U_1\,. \tag{3}$$

In the vicinity of the threshold the reaction is dominated by the following partonic subprocesses

$$\begin{aligned} q(k_1) + \bar{q}(k_2) &\to t(p_1) + X[\bar{t}](p_2')\,,\\ g(k_1) + g(k_2) &\to t(p_1) + X[\bar{t}](p_2')\,, \end{aligned} \tag{4}$$

where the initial-state parton momenta expressed in terms of momentum fractions x_1, x_2 are $k_1 = x_1 P_1$ and $k_2 = x_2 P_2$. The recoil momentum $p_2' = p_2 + k$ accounts for momentum p_2 at the threshold and any additional radiation indicated by momentum k.

In the vicinity of the partonic threshold, the hadronic final state $X[\bar{t}(p_2')] \equiv \bar{t}(p_2)$ and the anti-top carries momentum p_2. The Mandelstam invariants at parton level are defined as

$$\begin{aligned} &s = x_1 x_2 S = (k_1+k_2)^2\,,\ t_1 = x_2 T_1 = (k_2-p_1)^2 - m_t^2\,,\\ &u_1 = x_1 U_1 = (k_1-p_1)^2 - m_t^2\,,\ s_4 = s + t_1 + u_1\,, \end{aligned} \tag{5}$$

where the inelasticity of the reaction is accounted for by the invariant $s_4 = p_2'^2 - m_t^2$.

The factorized differential cross section is written as

$$\begin{aligned} S^2 \frac{d^2\sigma(S,T_1,U_1)}{dT_1\ dU_1} \;=\; &\sum_{i,j=q,\bar{q},g} \int_{x_1^-}^1 \frac{dx_1}{x_1} \int_{x_2^-}^1 \frac{dx_2}{x_2} f_{i/H_1}(x_1,\mu_F^2) f_{j/H_2}(x_2,\mu_F^2)\\ &\times \omega_{ij}(s,t_1,u_1,m_t^2,\mu_F^2,\alpha_s(\mu_R^2)) + \mathcal{O}(\Lambda^2/m_t^2) \end{aligned} \tag{6}$$

where $f_{j/H}(x,\mu_F^2)$ is the probability of finding the parton j in hadron H, μ_F and μ_R are the factorization and renormalization scales respectively, and ω_{ij} is the hard scattering cross section which depends on the kinematic of the reaction. Power suppressed terms Λ^2/m_t^2 are neglected here. The integration limits in the factorization formula are given by

$$x_1^- = -\frac{U_1}{S+T_1}\,,\quad x_2^- = -\frac{x_1 T_1}{x_1 S + U_1}. \tag{7}$$

[2]The extension of DIFFTOP to calculate approximate NNLO differential cross section for PIM kinematic is under development.

The double-differential cross section in Eq.(6) can be expressed in terms of the transverse momentum p_T^t of the top quark and its rapidity y by observing that

$$T_1 = -\sqrt{s}\; m_T e^{y}\,, \quad U_1 = -\sqrt{s}\; m_T e^{-y}\,, \tag{8}$$

where the transverse mass m_T is defined as $m_T = \sqrt{p_T^2 + m_t^2}$.

According to QCD resummation, in the organization of the large logarithms at the threshold of the heavy system, the hard scattering ω_{ij} functions are expanded in terms of singular functions which are plus-distributions of the type [3]

$$\left[\frac{\ln^l\left(s_4/m_t^2\right)}{s_4}\right]_+ = \lim_{\Delta\to 0}\left\{\frac{\ln^l\left(s_4/m_t^2\right)}{s_4}\theta(s_4-\Delta) + \frac{1}{l+1}\ln^{l+1}\left(\frac{\Delta}{m_t^2}\right)\delta(s_4)\right\}\,, \tag{9}$$

where corrections are denoted as leading-logarithmic (LL) if $l = 2i+1$ at $\mathcal{O}(\alpha_s^{i+3})$ with $i = 0, 1, \ldots$, as next-to-leading logarithm (NLL) if $l = 2i$, as next-to-next-to-leading logarithm (NNLL) if $l = 2i-1$, and so on.

Since QCD threshold resummation calculations and resummed formulae for inclusive cross sections for heavy-quark pair production have been extensively discussed in the literature in the past years, we will omit explicit derivations unless necessary and limit ourselves to general definitions. The calculation implemented in DIFFTOP strictly follows the derivation of Ref. [55] and references therein, which we refer to for details. Other particulars of this calculation can be found in [54, 56, 58, 76].

3 Overview of the threshold resummation calculation

As described in [52, 55] the fully resummed expression for the hard scattering cross section of Eq.(6) in 1PI kinematic is given by a trace in the color-tensor space of operators in the Mellin N-moment space

$$\begin{aligned}
&\omega_{ij}[N, s, t_1, u_1, m_t^2, \mu_R^2, \mu_F^2, \alpha_s(\mu_R)] = \mathrm{Tr}\left\{H_{ij}(s_4, t_1, u_1, m_t^2, \mu_R^2, \mu_F^2)\right.\\
&\times\overline{P}\exp\left[\int_{m_t}^{m_t/N}\frac{d\mu}{\mu}(\Gamma_S^{ij})^\dagger(\alpha_s(\mu))\right] S_{ij}(s_4, t_1, u_1, m_t^2, \mu_R^2, \mu_F^2)\\
&\left.\times P\exp\left[\int_{m_t}^{m_t/N}\frac{d\mu}{\mu}\Gamma_S^{ij}(\alpha_s(\mu))\right]\right\}\exp\left[E_i(N_u, m_t, \mu_F, \mu_R)\right]\exp\left[E_j(N_t, m_t, \mu_F, \mu_R)\right]\\
&\times\exp\left\{2\int_{\mu_R}^{m_t}\frac{d\mu}{\mu}\left[\gamma_i(\alpha_s(\mu)) + \gamma_j(\alpha_s(\mu))\right]\right\}\,,
\end{aligned} \tag{10}$$

where $N_u = N(-u_1/m_t^2)$, $N_t = N(-t_1/m_t^2)$ are the Mellin moments in 1PI kinematic. The functions $H_{ij} = H_{ij}^{(0)} + (\alpha_s/\pi)H_{ij}^{(1)} + \cdots$ and $S_{ij} = S_{ij}^{(0)} + (\alpha_s/\pi)S_{ij}^{(1)} + \cdots$ are the hard and soft

[3] This logarithmic structure refers to the 1PI kinematic. In PIM kinematic one has $\left[\ln^l(1-z)/(1-z)\right]_+$, where $z = M^2/s$ and M is the invariant mass of the final-state heavy system.

functions respectively. The functions $\Gamma_S = (\alpha_s/\pi)\Gamma_S^{(1)} + (\alpha_s/\pi)^2\Gamma_S^{(2)} + \cdots$ are the soft anomalous dimension matrices which are path-ordered in μ. Finally, $\gamma_i = (\alpha_s/\pi)\gamma_i^{(1)} + (\alpha_s/\pi)^2\gamma_i^{(2)} + \cdots$ are the anomalous dimensions of the quantum field $i = q, g$. In our calculation, $\Gamma_S^{(2)}$ at two-loop for the massive case (see e.g. [77, 78]) is included.

The exponentials $\exp E_i$ and $\exp E_j$ represent resummed expressions for the collinear and soft radiation from incoming and outgoing partons respectively, and are defined as

$$\begin{aligned} \exp\left[E_i(N_u, m_t, \mu_F, \mu_R)\right] &= \exp\left\{E_i(N_u, 2k_i\cdot\zeta)\right\} \\ &\times \exp\left\{-2\int_{\mu_R}^{2k_i\cdot\zeta}\frac{d\mu}{\mu}\gamma_i(\alpha_s(\mu)) + 2\int_{\mu_F}^{2k_i\cdot\zeta}\frac{d\mu}{\mu}\gamma_{i/i}(N_u, \alpha_s(\mu))\right\}, \end{aligned} \tag{11}$$

where $\gamma_{i/i}$ are the anomalous dimensions of the operator whose matrix element represents the parton density $f_{i/i}$ in the $\overline{\rm MS}$ scheme. The vector $\zeta = p_2/m_t$ is used to define the distance from the threshold in 1PI kinematic: $s_4/m_t^2 \approx 2(\zeta\cdot k)/m_t$. The first exponential in Eq.(11) is defined as

$$\begin{aligned} E_i(N, 2k_i\cdot\zeta) &= \int_0^\infty dw \frac{(1-e^{-Nw})}{w} \\ &\times \left\{\int_{w^2}^1 \frac{d\lambda}{\lambda} A_i[\alpha_s(\sqrt{\lambda}\; 2k_i\cdot\zeta)] + \frac{1}{2}\nu^i[\alpha_s(w\; 2k_i\cdot\zeta)]\right\}, \end{aligned} \tag{12}$$

where functions A_i and ν^i have perturbative expansion in α_s whose explicit expressions up to $\mathcal{O}(\alpha_s^2)$ can be found in [55, 76] for the Feynman and axial gauge.

After an α_s-expansion of the resummed hard-scattering cross section, the general structure of the double-differential cross section at parton level is given by

$$s^2\frac{d\sigma_{ij}(s, t_1, u_1, \mu_R, \mu_F)}{dt_1\; du_1} = \omega_{ij}^{(0)}(s_4, s, t_1, u_1) + \frac{\alpha_s}{\pi}\omega_{ij}^{(1)}(s_4, s, t_1, u_1) + \left(\frac{\alpha_s}{\pi}\right)^2\omega_{ij}^{(2)}(s_4, s, t_1, u_1), \tag{13}$$

where $\omega_{ij}^{(0)}$ is the cross section at the Born level and the one-loop soft-gluon correction beyond the LL approximation can be written as

$$\begin{aligned} \omega_{ij}^{(1)}(s_4, s, t_1, u_1) &= C_1^{(1)}\left[\frac{\ln(s_4/m_t^2)}{s_4}\right]_+ + \left(C_0^{(1)} + C_{0,\mu_F}^{(1)}\right)\ln\left(\frac{\mu_F^2}{m_t^2}\right)\left[\frac{1}{s_4}\right]_+ \\ &+ \left[R_1 + r_{1,\mu_F}\ln\left(\frac{\mu_F^2}{m_t^2}\right) + r_{1,\mu_R}\ln\left(\frac{\mu_R^2}{m_t^2}\right)\right]\;\delta(s_4), \end{aligned} \tag{14}$$

where coefficients $C_0^{(1)}, C_1^{(1)}$ (in which we suppress the ij indices) and r_1 can be found in Appendix B of [55]. At the NNLL accuracy the coefficient R_1 which consists of virtual graph and soft-gluon radiation contributions, contains the NLO matching term $\mathrm{Tr}\left[H^{(0)}S^{(1)} + H^{(1)}S^{(0)}\right]$. The expression of the NLO matching term is that of the soft plus virtual $(S+V)$ contributions in Eq.(6.19) of Ref. [17] for the gg channel, and that of the contributions in Eq.(4.7) of Ref. [19]

for the $q\bar{q}$ channel. The Coulomb interactions, due to gluon exchange between the final-state heavy quarks, are included at 1-loop level.

The two-loop corrections at the NNLL accuracy can be written as

$$\begin{aligned}
\omega_{ij}^{(2)}(s_4,s,t_1,u_1) &= C_3^{(2)}\left[\frac{\ln^3(s_4/m_t^2)}{s_4}\right]_+ + \left[C_2^{(2)} + C_{2,\mu_F}^{(2)}\ln\left(\frac{\mu_F^2}{m_t^2}\right)\right]\left[\frac{\ln^2(s_4/m_t^2)}{s_4}\right]_+ \\
&+ \left[C_1^{(2)} + C_{1,\mu_F}^{(2)}\ln\left(\frac{\mu_F^2}{m_t^2}\right) + C_{1,\mu_R}^{(2)}\ln\left(\frac{\mu_R^2}{m_t^2}\right) + \overline{C}_{1,\mu_F}^{(2)}\ln^2\left(\frac{\mu_F^2}{m_t^2}\right)\right]\left[\frac{\ln(s_4/m_t^2)}{s_4}\right]_+ \\
&+ \left[C_0^{(2)} + C_{0,\mu_F}^{(2)}\ln\left(\frac{\mu_F^2}{m_t^2}\right) + C_{0,\mu_R}^{(2)}\ln\left(\frac{\mu_R^2}{m_t^2}\right)\right. \\
&\quad \left. + \overline{C}_{0,\mu_F}^{(2)}\ln^2\left(\frac{\mu_F^2}{m_t^2}\right) + \overline{C}_{0,\mu_F,\mu_R}^{(2)}\ln\left(\frac{\mu_F^2}{m_t^2}\right)\ln\left(\frac{\mu_R^2}{m_t^2}\right)\right]\left[\frac{1}{s_4}\right]_+ \\
&+ \left[R_2 + r_{2,\mu_R}\ln\left(\frac{\mu_R^2}{m_t^2}\right) + r_{2,\mu_F}\ln\left(\frac{\mu_F^2}{m_t^2}\right) + r_{2,\mu_F,\mu_R}\ln\left(\frac{\mu_F^2}{m_t^2}\right)\ln\left(\frac{\mu_R^2}{m_t^2}\right)\right. \\
&\quad \left. + \overline{r}_{2,\mu_R}\ln^2\left(\frac{\mu_R^2}{m_t^2}\right) + \overline{r}_{2,\mu_F}\ln^2\left(\frac{\mu_F^2}{m_t^2}\right)\right]\ \delta(s_4)\,, \qquad (15)
\end{aligned}$$

where again, explicit expressions for the coefficients $C_{0,\mu_F}^{(2)}, C_1^{(2)}, \ldots$ can be found in Appendix B of [55]. In the current implementation the scale-independent coefficient $C_0^{(2)}$ contains the contribution from the soft anomalous dimension $\Gamma_S^{(2)}$ plus process-independent terms [57, 76] which are universal in the $q\bar{q}$ and gg channels respectively. These contributions are formally at the next-to-next-to-next-leading logarithmic (NNNLL) accuracy. In the scale-independent coefficient R_2 we only include NNNLL subleading terms coming from moment to momentum space inversion [54]. The full knowledge of R_2 requires matching conditions at NNLO which include explicit analytical expressions for $H^{(2)}$ and $S^{(2)}$. Explicit expressions in SCET for $S^{(2)}$ in PIM kinematic, in the limit of boosted top quarks, can be found in Ref. [71]. Related studies are presented in Refs. [28, 29, 71, 79–81].

By setting $\mu_R = \mu_F = \mu$ one can write the inclusive total partonic cross section in terms of scaling functions $f_{ij}^{(k,l)}$ that are dimensionless and depend only on the variable $\eta = s/(4m_t^2) - 1$

$$\sigma_{ij}(s, m_t^2, \mu^2) = \frac{\alpha_s^2(\mu)}{m_t^2}\sum_{k=0}^{\infty}\left(4\pi\alpha_s(\mu)\right)^k \ \sum_{l=0}^{k} f_{ij}^{(k,l)}(\eta)\ln^l\left(\frac{\mu^2}{m_t^2}\right). \qquad (16)$$

To reduce the impact of threshold logarithms in the large-η regions of the scaling functions we made use of dumping factors as it is done in Ref. [18].

4 Phenomenological analysis

In this section we present details of the phenomenological analysis. DiffTop predictions are confronted to the recent measurements of differential distributions for $t\bar{t}$ production at $\sqrt{S} = 7$ TeV by the CMS [10] and ATLAS [13] collaborations. The theoretical systematic uncertainties associated to variations of PDFs, $\alpha_s(M_Z)$, scale, and m_t, are investigated individually. In

particular, transverse momentum p_T^t and rapidity y^t distributions of the final state top-quark, measured by CMS, and the p_T^t distribution by ATLAS[4] are studied. Our central prediction is the approximate NNLO + NNLL as defined above. The on-shell pole-mass definition for the top-quark mass is used, and the value of $m_t = 173$ GeV is chosen. The scales are set to $\mu_F = \mu_R = m_t$. The experimental measurements published by CMS and ATLAS are differential distributions that are normalized to the total cross section in bins of p_T^t and y^t. This representation of experimental data is motivated by (partial) cancellation of systematic uncertainties. However, this type of measurement has limitations, which will be discussed later.

The correlation between the p_T^t distribution for $t\bar{t}$ production at the LHC at $\sqrt{S} = 7$ TeV and the gluon, as a function of x of the gluon ($x_{\rm gluon}$) is illustrated in Fig. 2. A strong correlation is observed at $x_{\rm gluon} \approx 0.1$. Here, the p_T^t distribution is averaged in 4 bins and the correlation cosine $\cos\phi$, as defined in [82], is evaluated for each bin. The predictions using MSTW08 [83] (left) and CT10 [84] (right) PDFs at NNLO are shown here, while those using ABM11 [85], HERAPDF1.5 [86], and NNPDF2.3 [87] have similar behaviors.

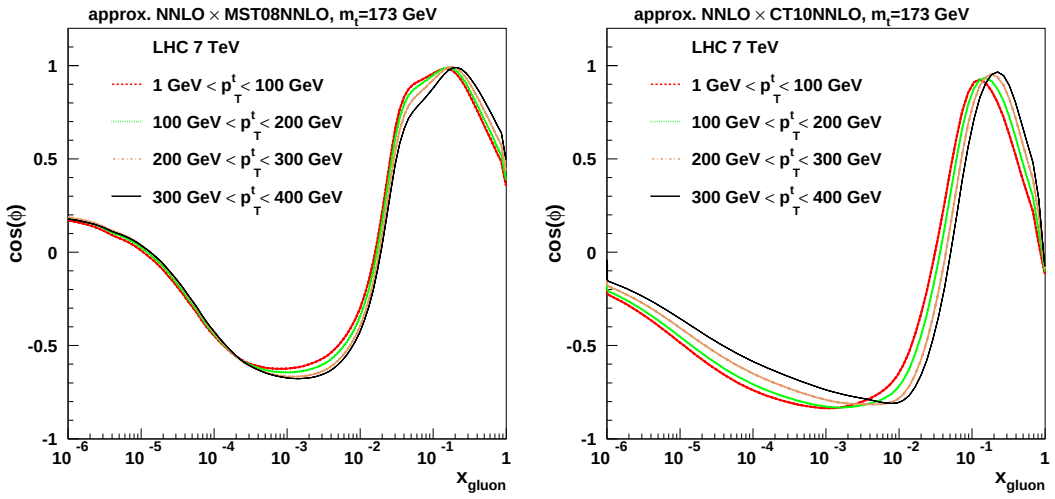

Figure 2: Theoretical correlation cosine as a function of $x_{\rm gluon}$ for the p_T^t distribution in $t\bar{t}$ production at the LHC at $\sqrt{S} = 7$ TeV. MSTW08 (left) and CT10 (right) PDFs at NNLO are used. Different lines represent each p_T^t bin.

The uncertainties associated to the various PDFs are computed by using the prescription given by each PDF group. All envelopes represent the 68% confidence level (CL). For the CT10 case, being the CT10NNLO PDF given at 90% CL, the asymmetric PDF errors are rescaled by a factor 1.642. In the ABM11 case, the total uncertainty obtained by using the symmetric formula for the eigenvector sets, represents the PDF + α_s uncertainty at the 68% CL. The uncertainty of HERAPDF1.5 NNLO is determined by including the experimental (at the 68% CL), model

[4]In the data set we considered, y^t is not provided by the ATLAS collaboration.

and parametrization uncertainties, which are summed in quadrature to obtain the total error.

The uncertainty associated to the variations of $\alpha_s(M_Z)$ is computed by using the central $\alpha_s(M_Z)$ values given by each PDF group, and by considering up- and down-variations $\Delta\alpha_s(M_Z) = \pm 0.001$. This is more conservative with respect to the 68% CL variation $\Delta\alpha_s(M_Z) = 0.0007$, reported in the PDG 2012 [88]. The central values for $\alpha_s(M_Z)$ provided by the different PDF groups are: 0.1134, 0.118, 0.1176, 0.1171, 0.118 for ABM11 [85], CT10 [84], HERAPDF1.5 [86], MSTW08 [83], and NNPDF2.3 [87], respectively. The HERAPDF1.5 $\alpha_s(M_Z)$ uncertainty is obtained by varying $0.1170 \leq \alpha_s(M_Z) \leq 0.1190$, resulting in a larger uncertainty on the cross section, as compared to the other PDF sets[5].

The uncertainty related to the choice of the scale has been estimated by varying $m_t/2 \leq \mu_R = \mu_F \leq 2m_t$. As shown in Fig. 1, where the approximate NNLO prediction and the full NLO calculation obtained by MCFM [37] are compared, the reduction of the scale dependence is substantial. When these theory predictions are compared to the LHC data for the p_T^t distribution, the shape is also modified when passing from NLO to NNLO. In the NNLO case, the theoretical description of the measurements is significantly improved.

The uncertainty associated to the pole mass m_t has been assessed by considering variations $\Delta m_t = \pm 1$ GeV around the central value $m_t = 173$ GeV.

5 Results

In Tab. 1 we summarize the results for the $t\bar{t}$ total inclusive cross section at the LHC at $\sqrt{S}$ =7 TeV for each PDF set with relative uncertainties. The total uncertainty on the theory prediction is dominated by the PDF errors ($\approx 3-5\%$) and uncertainty related to variations of m_t ($\approx 3\%$). The spread of the central values is mostly due to the fact that the parton luminosities are driven by different gluon PDFs from each group. These differences arise from the different methodologies and inputs (heavy-flavor treatment, values of $\alpha_s(M_Z)$, data selection, etc.) adopted by each PDF fitting group in their QCD analyses. Experimental, parametrization, and model uncertainties for HERAPDF1.5 have been reported separately. The inclusion of the model uncertainty results in an increase of the cross section by approximately 20%, related to the variation of the q^2 cut on the used DIS data. The α_s variation attributed to ABM11 is already included in the quoted PDF error since in the ABM fit α_s is simultaneously determined together with the PDFs.

In Figs. 3-7 we illustrate the main results of our phenomenological analysis for each PDF set separately, and present the approximate NNLO predictions for absolute p_T^t and y^t distributions. In each figure, we show the individual uncertainty due to variations of PDFs, $\alpha_s(M_Z)$, scales, and

[5]The variation corresponding to the inclusion of members 9-11 of the HERAPDF1.5 α_s sets gives an increased uncertainty of approximately $\pm 6.3\%$.

LHC 7 TeV $m_t = 173$ GeV					
PDF set	$\sigma_{t\bar{t}}$ [pb]	δ_{PDF} [pb]	δ_{α_s} [pb]	δ_{scale} [pb]	δ_{m_t} [pb]
ABM11	140.9	$^{+6.4}_{-6.4}$ $(^{+4.5\%}_{-4.5\%})$	$^{+0.0}_{-0.0}$	$^{+0.0}_{-1.8}$ $(^{+0.0\%}_{-1.3\%})$	$^{+4.0}_{-4.8}$ $(^{+2.8\%}_{-3.4\%})$
CT10	180.3	$^{+8.7}_{-7.0}$ $(^{+4.8\%}_{-3.9\%})$	$^{+4.5}_{-4.5}$ $(^{+2.5\%}_{-2.5\%})$	$^{+3.3}_{-4.4}$ $(^{+1.8\%}_{-2.4\%})$	$^{+5.0}_{-5.9}$ $(^{+2.8\%}_{-3.3\%})$
HERA1.5	185.2	$^{+4.2}_{-6.7^{exp}}$ $(^{+2.3\%}_{-3.6\%})$ $^{+0.03}_{-6.8^{par}}$ $(^{+3.7\%}_{-0.0\%})$ $^{+39.3}_{-5.9^{mod}}$ $(^{+21.2\%}_{-3.1\%})$	$^{+5.9}_{-5.9}$ $(^{+3.2\%}_{-3.2\%})$	$^{+3.2}_{-2.5}$ $(^{+1.7\%}_{-1.3\%})$	$^{+5.1}_{-6.0}$ $(^{+2.7\%}_{-3.2\%})$
MSTW08	179.4	$^{+4.9}_{-5.0}$ $(^{+2.7\%}_{-2.8\%})$	$^{+4.3}_{-4.3}$ $(^{+2.4\%}_{-2.4\%})$	$^{+3.3}_{-4.4}$ $(^{+1.8\%}_{-2.4\%})$	$^{+5.0}_{-5.8}$ $(^{+2.8\%}_{-3.2\%})$
NNPDF23	179.9	$^{+5.5}_{-5.5}$ $(^{+3.0\%}_{-3.0\%})$	$^{+3.7}_{-3.7}$ $(^{+2.0\%}_{-2.0\%})$	$^{+3.3}_{-4.7}$ $(^{+1.8\%}_{-2.6\%})$	$^{+5.0}_{-6.0}$ $(^{+2.8\%}_{-3.3\%})$

Table 1: Values of the total inclusive $t\bar{t}$ cross section with corresponding uncertainties for PDFs, $\alpha_s(M_Z)$, scale dependence and m_t.

m_t, each indicated by a band of different style.[6] The total uncertainty is obtained by summing all these contributions in quadrature and is represented by a shaded band. Also, we show p_T^t and y^t normalized distributions divided by the CMS and ATLAS data. Again, different contributions to the theory uncertainty are presented individually, and the total uncertainty is shown by a light shaded band. At large p_T^t and $|y^t|$, where regions of larger values of x are probed, the PDF uncertainties increase since the gluon distribution in this range is poorly constrained at present.

Variations of m_t modify magnitude and shape of large-p_T distribution and represent the second dominant uncertainty. This reflects the strong sensitivity of differential distributions to the top-quark mass.

In some regions of the p_T^t and y^t spectra, the uncertainty associated to variations of $\alpha_s(M_Z)$ is larger than that related to scale variation. The usage of the $\overline{\text{MS}}$ scheme definition for the top-quark mass in the calculation is expected to improve the convergence of perturbation theory and, in turn, to reduce the scale dependence [89].

When theory predictions are compared to the data, CMS and ATLAS measurements exhibit some differences in the shape of the normalized p_T^t distribution, in particular in the first and third bin. In general, the first bins of transverse momentum $0 \leq p_T^t \leq 200$ GeV and central bins of rapidity $-1.5 \leq y^t \leq 1.5$ have potentially more constraining power, because of smaller experimental uncertainties.

In Fig. 8 predictions for the absolute p_T^t and y^t distributions are shown, with all used PDF sets compared within the respective total uncertainties, represented by bands with different hatches. The predictions using ABM11 are found to be generally lower with respect to the other sets, because different methodologies used in the ABM11 analysis lead to a lower gluon and smaller $\alpha_s(M_Z)$ value. Agreement of the prediction using ABM11 with that using other PDF sets can be achieved by choosing a smaller value of the top-quark pole mass within the current uncertainties, see, e.g., [90].

In Fig. 9 we compare predictions using different PDF sets to the CMS and ATLAS data.

[6]The absolute p_T^t and y^t distributions are calculated by using 45 grid points to balance the size of the FastNLO tables and the necessary CPU time to produce such tables. A larger number of grid points (70-80) results in much smoother curves and all conclusions remain unchanged.

As in Fig. 8, errors for the different PDF sets are represented by bands with different hatches. At the present stage, even though the CMS and ATLAS measurements exhibit relatively large uncertainties, these data might have some impact in PDFs determination once included in QCD fit analyses. On the other hand, a significant amount of information contained in the measurements of differential distributions is lost by normalizing the data. Measurements of absolute differential cross sections are of crucial importance to fully exploit the potential of the $t\bar{t}$ production to constrain the gluon distribution. Moreover, a reduction of the statistic and systematic uncertainties in the high-energy run of the LHC will be of clear advantage. The possibility of a finer binning at lower p_T^t should also be explored.

6 Summary and conclusions

Measurements of p_T^t and y^t differential cross sections in top-quark pair production in hadron collisions are going to play an important role in constraining the gluon PDF at large-x as the LHC will reach higher energies in the collisions in the forthcoming run II. Given the accuracy of the present data and the existing correlations between the strong coupling $\alpha_s(M_Z)$, top-quark mass, and gluon PDF, these measurements might have an impact in constraining the large-x gluon distribution once included in QCD fit of PDFs. In particular, investigations of absolute differential cross sections will bring complementary information related to the magnitude and other details of the distributions, which will be crucial to improve the constraining power of the experimental data.

We have presented results for the differential cross section of $t\bar{t}$ production at approximate NNLO that are of interest for phenomenological studies at hadron colliders. This calculation is implemented into the flexible computer code DiffTop which used in this analysis. We investigated details of the theoretical predictions generated by using different PDF sets in which individual uncertainties due to variations of PDFs, scale, α_s and m_t are analyzed and compared to the recent measurements by the CMS and ATLAS collaborations.

The theory framework and the computer program DiffTop will undergo further extensions related to the calculation of distributions in the PIM kinematic which is currently under development. The code has been interfaced to FastNLO for fast theory evaluations. It will be made publically available and will be useful in QCD analyses for PDFs determination.

Acknowledgments

We would like to thank Ben Pecjak for providing mathematica files with expressions to cross-check part of the results on the matching conditions. We would also like to thank Nick Kidonakis and Maria Aldaya for useful discussions. This work is supported in part by the "Initiative and Networking Fund of the Helmholtz Association (HGF) under the contract S0-072", by Deutsche

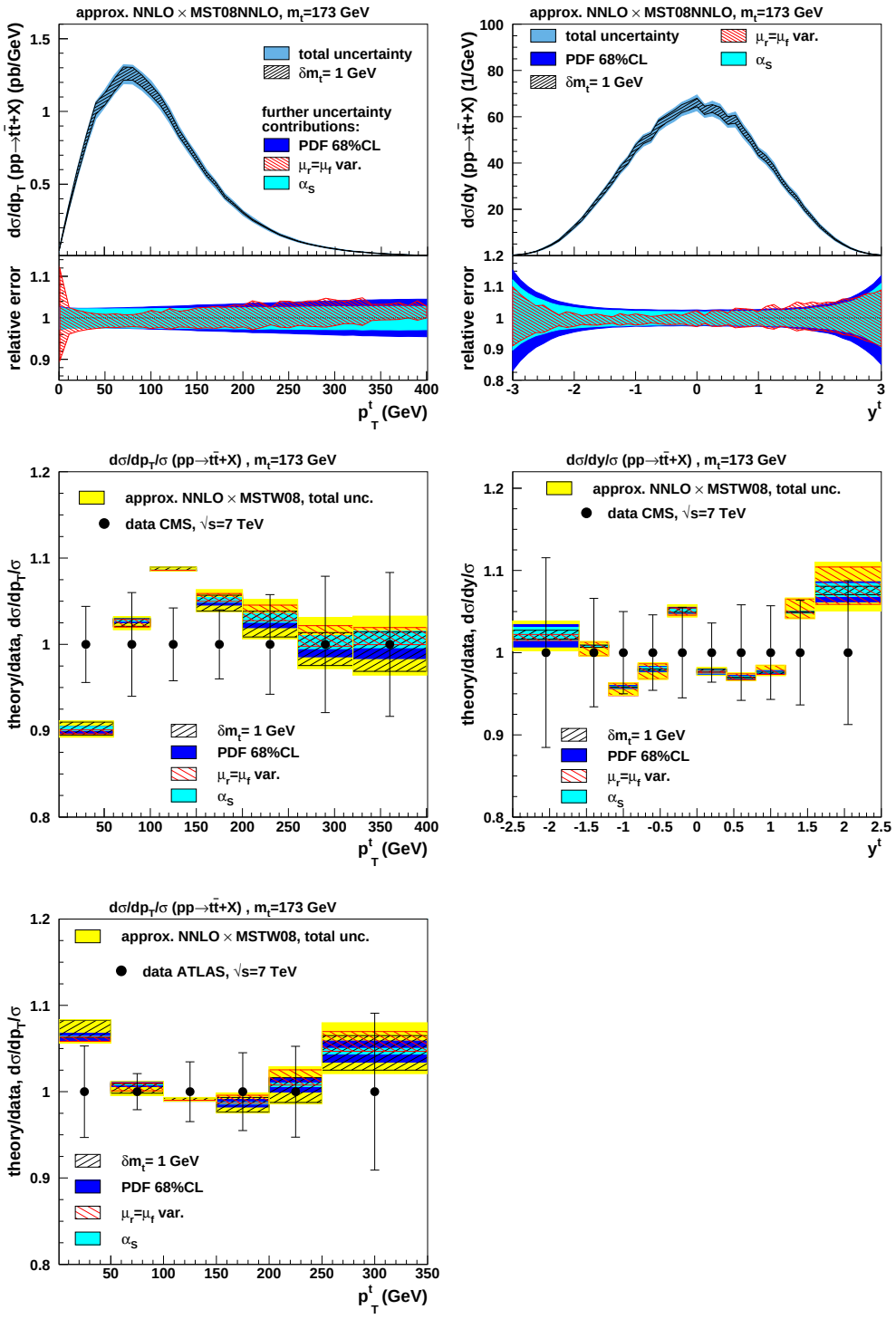

Figure 3: Upper inset: approx. NNLO predictions and the relative uncertainty for top-quark pair production cross sections as a function of p_T^t and y^t using MSTW08NNLO. Individual contributions of uncertainties due to PDF (68% CL), $\alpha_s(M_Z)$, scale and m_t variations are shown by bands of different shades. Lower inset: Ratio of theory over data (light shaded band) for p_T^t and y^t as compared to the LHC measurements (filled circles). The individual contributions of theory uncertainties are shown by bands of different shades.

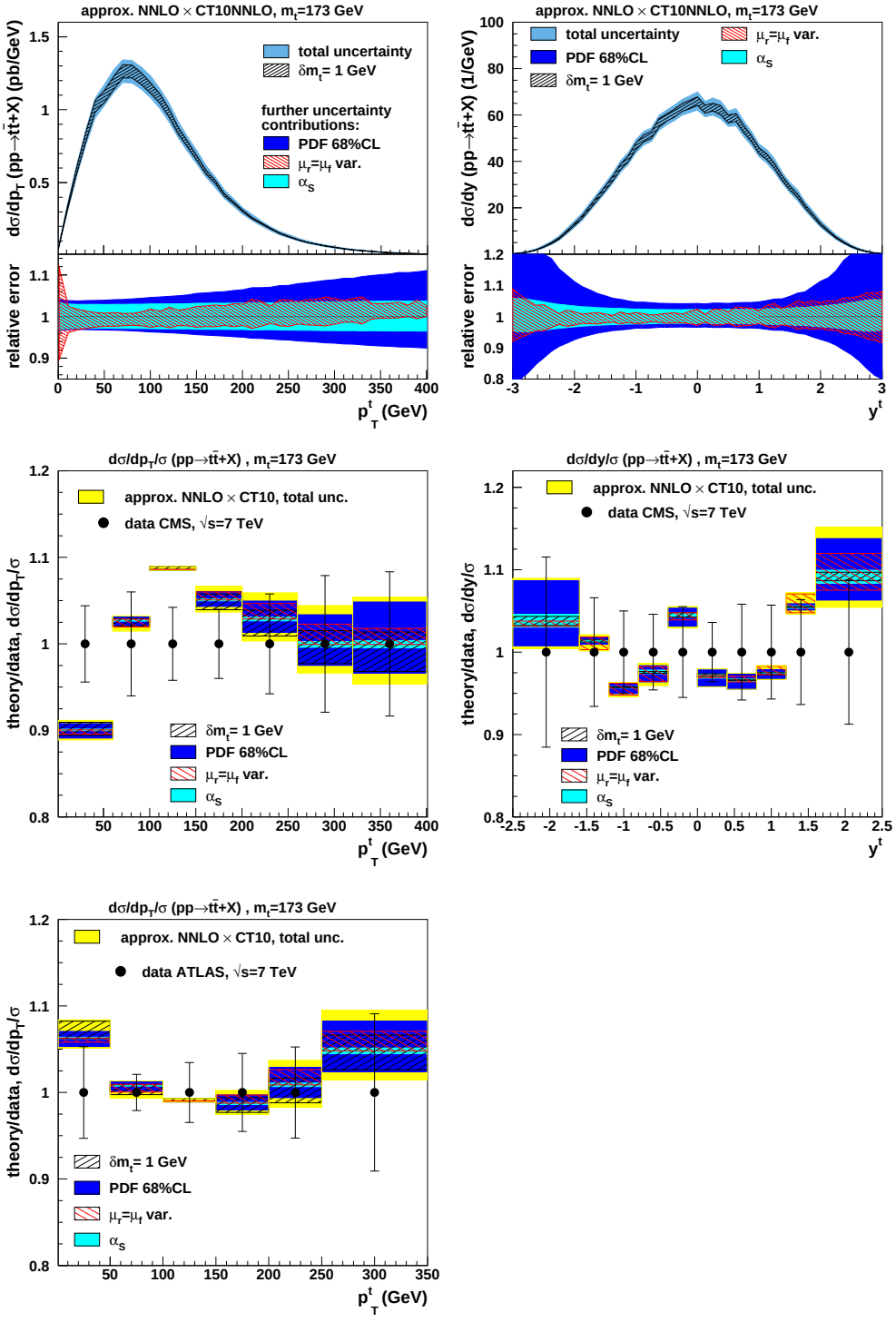

Figure 4: Same as in Fig. 3 using CT10NNLO PDFs.

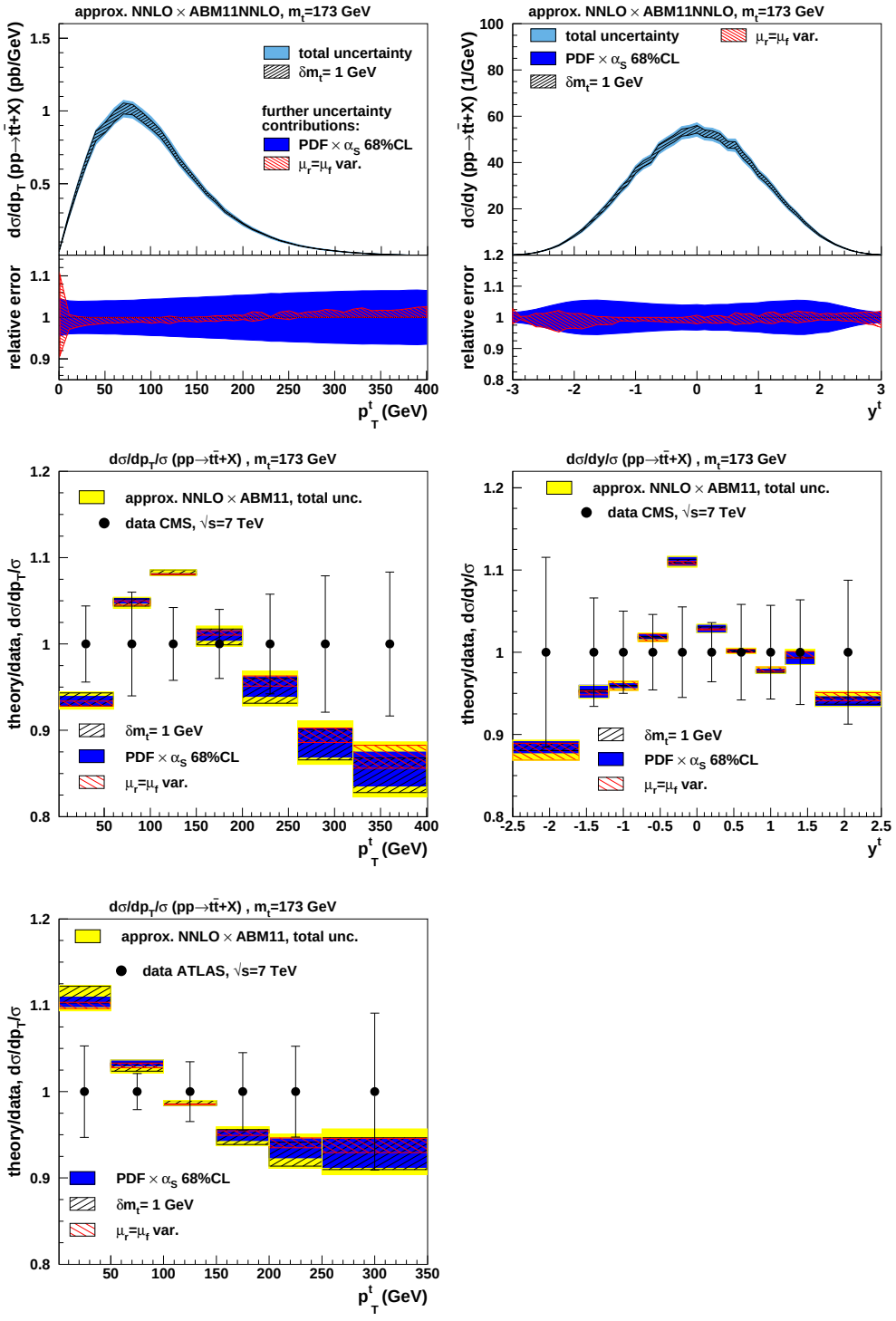

Figure 5: Same as in Fig. 3 using ABM11 PDFs. Here, the uncertainty on $\alpha_s(M_Z)$ is included into the PDF uncertainty, see description in the text.

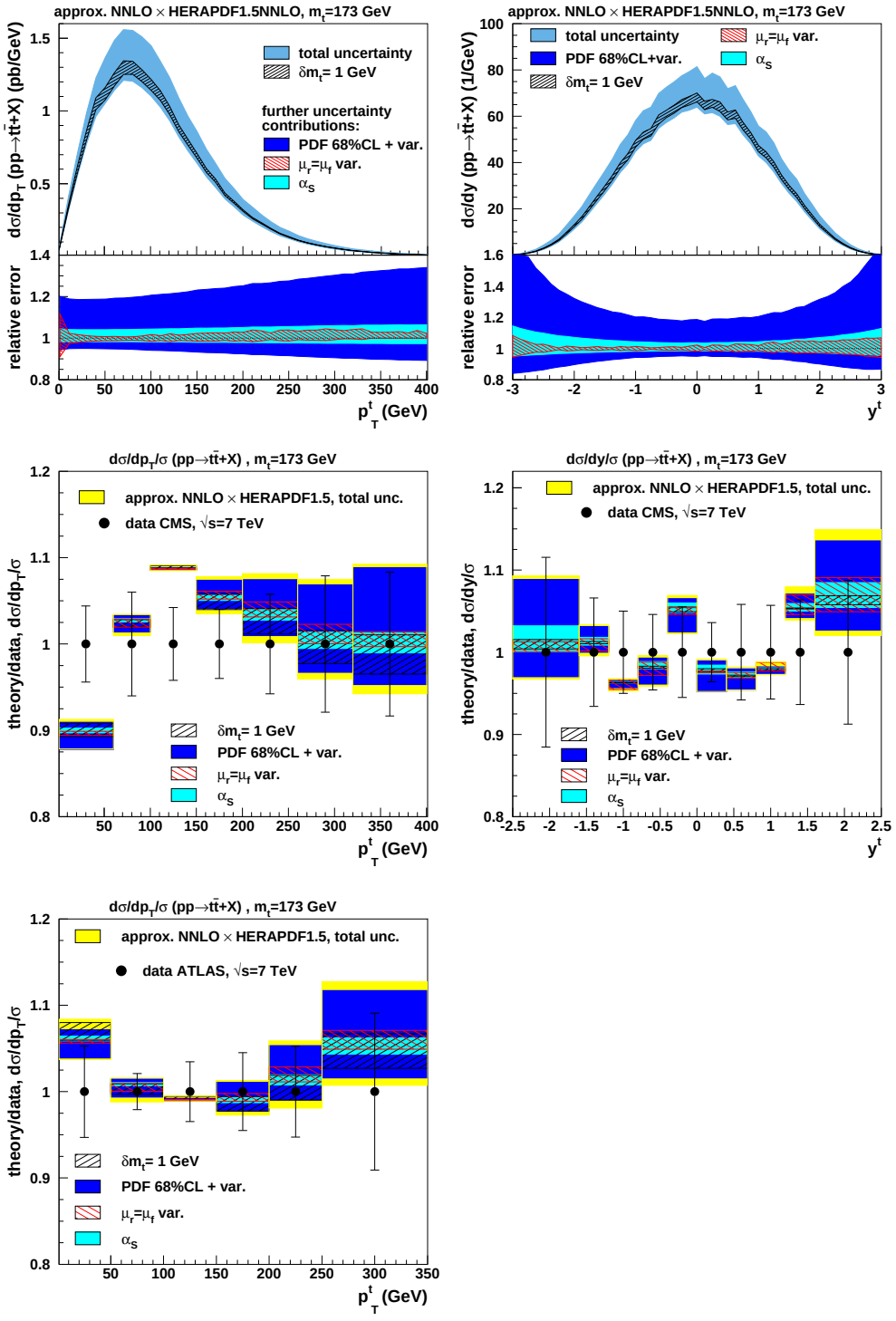

Figure 6: Same as in Fig. 3 using HERAPDF1.5 NNLO. The experimental uncertainties are given at 68% CL. In addition, model and parametrization uncertainties are considered.

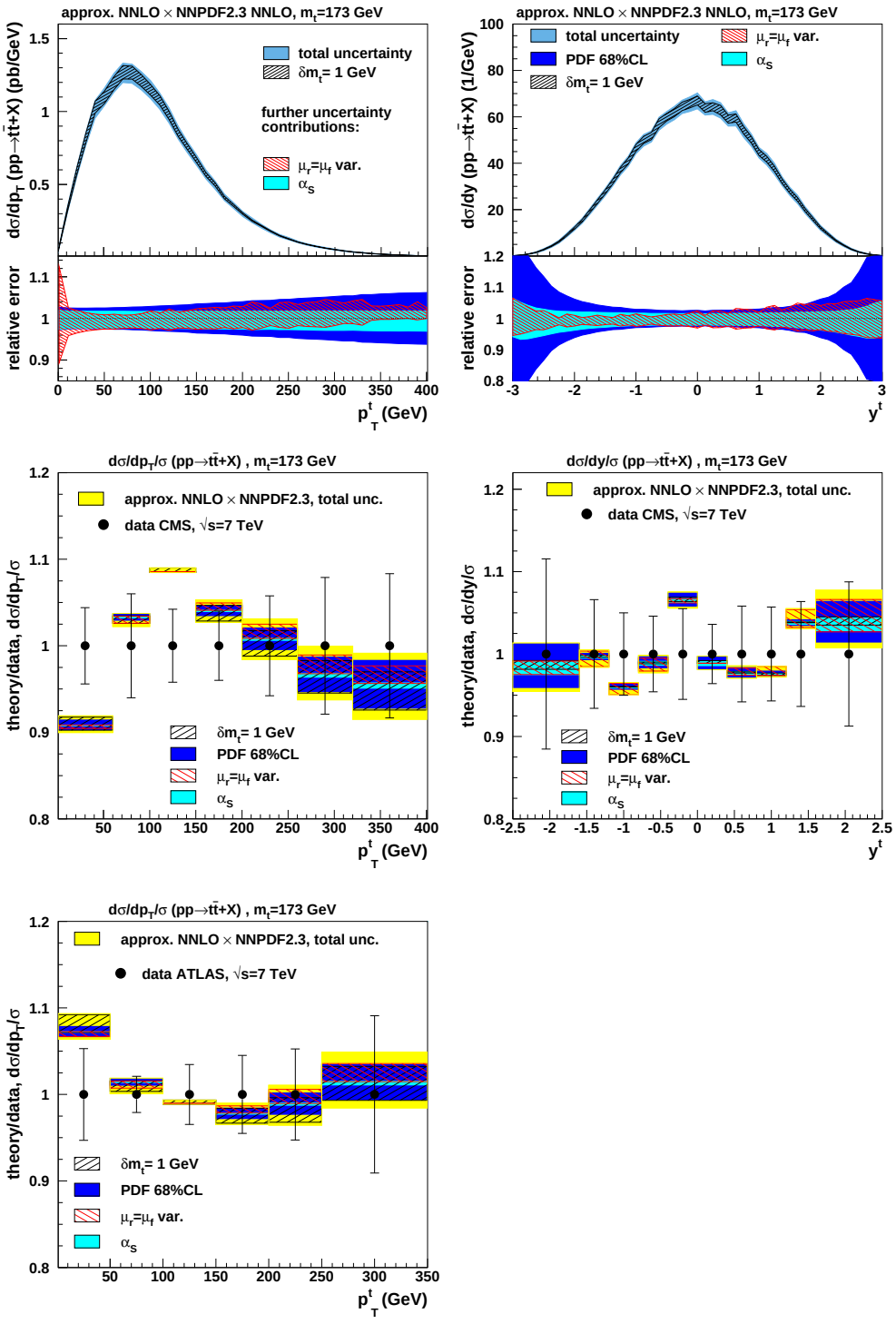

Figure 7: Same as in Fig. 3 using NNPDF2.3 PDFs.

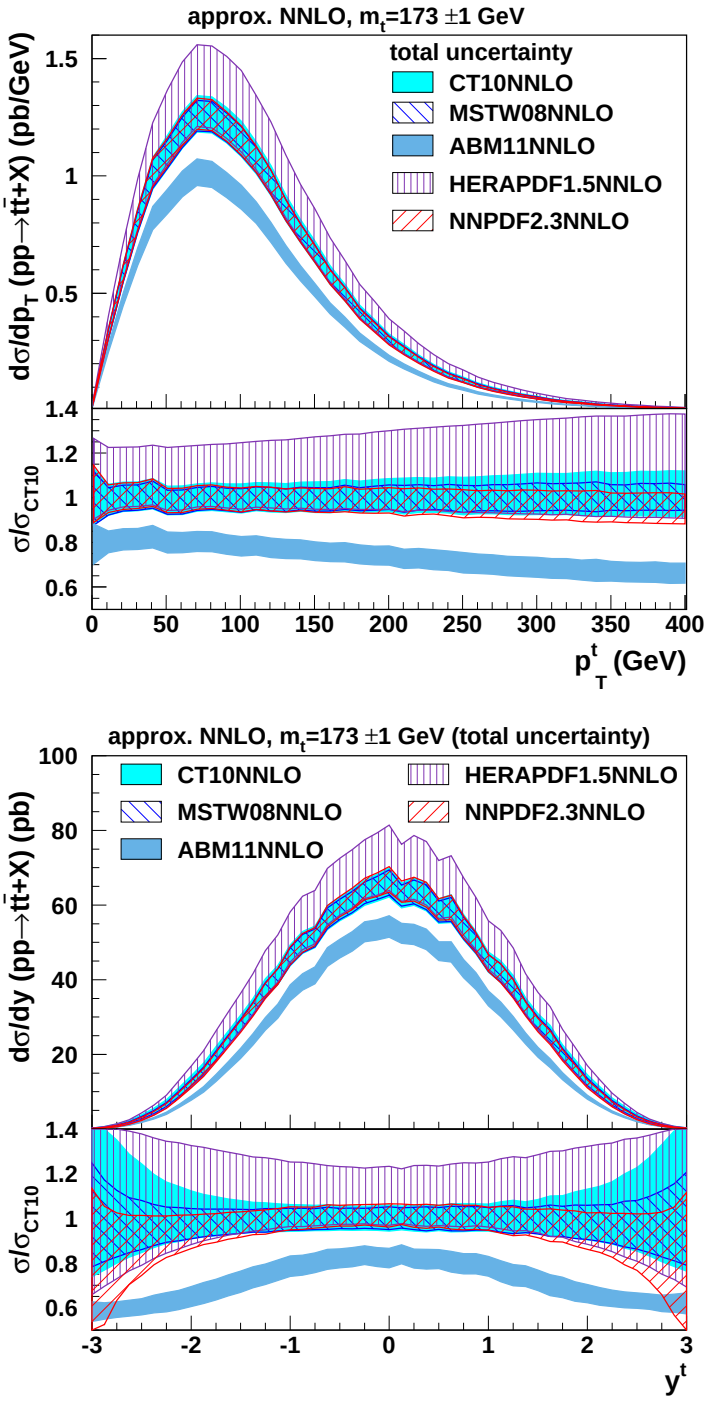

Figure 8: The approx. NNLO predictions for top-quark pair production cross sections at the LHC at $\sqrt{S} = 7$ TeV. Distributions of p_T^t (up) and y^t (low) are shown. Predictions, obtained by using different PDF sets are presented by bands of different hatches. The total uncertainty is obtained by summing the uncertainties due to PDFs, α_s, m_t and scale variations in quadrature.

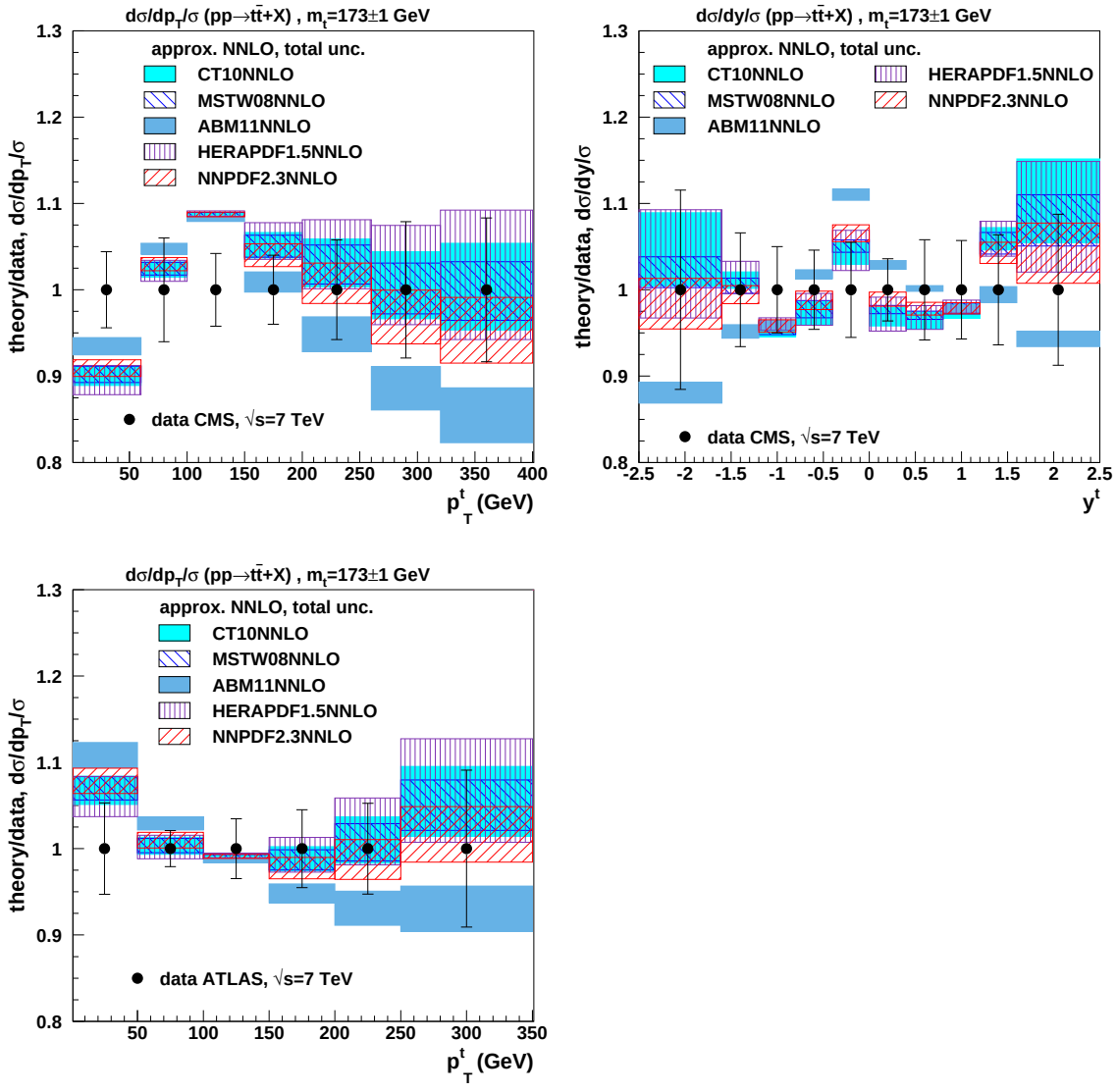

Figure 9: The approx. NNLO predictions for top-quark pair production at the LHC at $\sqrt{S} = 7$ TeV, shown as functions of p_T^t and y^t. The predictions, obtained by using different PDF sets are presented as a ratio to the LHC measurements (filled symbols). As in Fig. 8, error bands represent the total uncertainty.

Forschungsgemeinschaft in Sonderforschungsbereich/Transregio 9, by the European Commission through contract PITN-GA-2010-264564 (*LHCPhenoNet*), and it was realized within the scope of the PROSA collaboration.

References

[1] ATLAS Collaboration, G. Aad et al., Phys.Lett. B716 (2012) 1, 1207.7214.

[2] CMS Collaboration, S. Chatrchyan et al., Phys.Lett. B716 (2012) 30, 1207.7235.

[3] S. Alekhin, A. Djouadi and S. Moch, Phys.Lett. B716 (2012) 214, 1207.0980.

[4] F. Bezrukov, M.Y. Kalmykov, B. Kniehl and M. Shaposhnikov, JHEP 1210 (2012) 140, 1205.2893.

[5] ATLAS, CDF, CMS, and D0 Collaborations, (2014), 1403.4427.

[6] S. Moch, S. Weinzierl, S. Alekhin J. Blümlein, L. de la Cruz, S. Dittmaier, M. Dowling,J. Erler, J.R. Espinosa, J. Fuster, X. Garcia i Tormo, A.H. Hoang, A. Huss, S. Kluth, M. Mulders, A.S. Papanastasiou, J. Piclum, K. Rabbertz, C. Schwinn, M. Schulze, E. Shintani, P. Uwer and N. Zerf, (2014), 1405.4781.

[7] S. Alioli, P. Fernandez, J. Fuster, A. Irles, S.-O. Moch, P.Uwer and M.Vos, Eur.Phys.J. C73 (2013) 2438, 1303.6415.

[8] S. Biswas, K. Melnikov and M. Schulze, JHEP 1008 (2010) 048, 1006.0910.

[9] CMS Collaboration, S. Chatrchyan et al., Phys.Lett. B728 (2014) 496, 1307.1907.

[10] CMS Collaboration, S. Chatrchyan et al., Eur.Phys.J. C73 (2013) 2339, 1211.2220.

[11] CMS Collaboration, S. Chatrchyan et al., (2013), 1312.7582.

[12] ATLAS Collaboration, G. Aad et al., Eur.Phys.J. C73 (2013) 2261, 1207.5644.

[13] ATLAS collaboration, G. Aad et al., ATLAS-CONF-2013-099, ATLAS-COM-CONF-2013-114 (2013).

[14] ATLAS collaboration, G. Aad et al., ATLAS-CONF-2013-097, ATLAS-COM-CONF-2013-112 (2013).

[15] P. Nason, S. Dawson and R.K. Ellis, Nucl.Phys. B303 (1988) 607.

[16] P. Nason, S. Dawson and R.K. Ellis, Nucl.Phys. B327 (1989) 49.

[17] W. Beenakker, H. Kuijf, W.L. Van Neerven and J. Smith, Phys.Rev. D40 (1989) 54.

[18] R. Meng, G.A. Schuler, J. Smith and W.L. Van Neerven, Nucl.Phys. B339 (1990) 325.

[19] W. Beenakker, W.L. Van Neerven, R. Meng, G.A. Schuler and J. Smith, Nucl.Phys. B351 (1991) 507.

[20] M.L. Mangano, P. Nason and G. Ridolfi, Nucl.Phys. B373 (1992) 295.

[21] M. Czakon, P. Fiedler and A. Mitov, Phys.Rev.Lett. 110 (2013) 252004, 1303.6254.

[22] M. Czakon and A. Mitov, JHEP 1301 (2013) 080, 1210.6832.

[23] M. Czakon and A. Mitov, JHEP 1212 (2012) 054, 1207.0236.

[24] P. Bärnreuther, M. Czakon and A. Mitov, Phys.Rev.Lett. 109 (2012) 132001, 1204.5201.

[25] M. Czakon, A. Mitov and S. Moch, Nucl.Phys. B798 (2008) 210, 0707.4139.

[26] M. Czakon, A. Mitov and S. Moch, Phys.Lett. B651 (2007) 147, 0705.1975.

[27] A. Mitov and S. Moch, JHEP 0705 (2007) 001, hep-ph/0612149.

[28] A. Ferroglia, M. Neubert, B.D. Pecjak and L.-L. Yang, Phys.Rev.Lett. 103 (2009) 201601, 0907.4791.

[29] A. Ferroglia, M. Neubert, B.D. Pecjak and L.-L. Yang, JHEP 0911 (2009) 062, 0908.3676.

[30] M. Czakon, Phys.Lett. B693 (2010) 259, 1005.0274.

[31] I. Bierenbaum, M. Czakon and A. Mitov, Nucl.Phys. B856 (2012) 228, 1107.4384.

[32] P. Bärnreuther, M. Czakon and P. Fiedler, JHEP 1402 (2014) 078, 1312.6279.

[33] M. Aliev, H. Lacker, U. Langenfeld, S.O. Moch, P. Uwer and M. Wiedermann, Comput.Phys.Commun. 182 (2011) 1034, 1007.1327.

[34] A. Denner, S. Dittmaier, S. Kallweit and S. Pozzorini, Phys.Rev.Lett. 106 (2011) 052001, 1012.3975.

[35] G. Bevilacqua, M. Czakon, A. van Hameren, C.G. Papadopoulos and M. Worek, JHEP 1102 (2011) 083, 1012.4230.

[36] A. Denner, S. Dittmaier, S. Kallweit and S. Pozzorini, JHEP 1210 (2012) 110, 1207.5018.

[37] J.M. Campbell and R.K. Ellis, Phys.Rev. D62 (2000) 114012, hep-ph/0006304.

[38] S. Frixione, P. Nason and B.R. Webber, JHEP 0308 (2003) 007, hep-ph/0305252.

[39] S. Alioli, K. Hamilton, P. Nason, C. Oleari and Emanuele Re, JHEP 1104 (2011) 081, 1012.3380.

[40] J. Alwall, P. Demin, S. de Visscher, R. Frederix, M. Herquet, F. Maltoni, T. Plehn, D.L. Rainwater and T. Stelzer, JHEP 0709 (2007) 028, 0706.2334.

[41] R. Frederix, S. Frixione, F. Maltoni and T. Stelzer, JHEP 0910 (2009) 003, 0908.4272.

[42] M. Beneke, P. Falgari, S. Klein, J. Piclum, C. Schwinn, M. Ubiali and F. Yan, JHEP 1207 (2012) 194, 1206.2454.

[43] M. Czakon, M.L. Mangano, A. Mitov and J. Rojo, JHEP 1307 (2013) 167, 1303.7215.

[44] D. Britzger, T. Kluge, K. Rabbertz, F. Stober and M. Wobisch, DIS 2014 - XXII. International Workshop on Deep-Inelastic Scattering and Related Subjects, 2014, `http://indico.cern.ch/event/258017/session/1/contribution/202`.

[45] D. Britzger, K. Rabbertz, F. Stober and M. Wobisch, (2012) 217, 1208.3641.

[46] fastNLO Collaboration, M. Wobisch, D. Britzger, T. Kluge, K. Rabbertz and F. Stober, (2011), 1109.1310.

[47] T. Kluge, K. Rabbertz and M. Wobisch, (2006) 483, hep-ph/0609285.

[48] G.F. Sterman, Nucl.Phys. B281 (1987) 310.

[49] S. Catani and L. Trentadue, Nucl.Phys. B327 (1989) 323.

[50] S. Catani and L. Trentadue, Nucl.Phys. B353 (1991) 183.

[51] N. Kidonakis and G.F. Sterman, Nucl.Phys. B505 (1997) 321, hep-ph/9705234.

[52] E. Laenen, G. Oderda and G.F. Sterman, Phys.Lett. B438 (1998) 173, hep-ph/9806467.

[53] R. Bonciani, S. Catani, M.L. Mangano and P. Nason, Nucl.Phys. B529 (1998) 424, hep-ph/9801375.

[54] N. Kidonakis, Phys.Rev. D64 (2001) 014009, hep-ph/0010002.

[55] N. Kidonakis, E. Laenen, S.O. Moch and R. Vogt, Phys.Rev. D64 (2001) 114001, hep-ph/0105041.

[56] N. Kidonakis, Int.J.Mod.Phys. A19 (2004) 1793, hep-ph/0303186.

[57] N. Kidonakis and R. Vogt, Phys.Rev. D68 (2003) 114014, hep-ph/0308222.

[58] N. Kidonakis, Phys.Rev. D73 (2006) 034001, hep-ph/0509079.

[59] N. Kidonakis and R. Vogt, Phys.Rev. D78 (2008) 074005, 0805.3844.

[60] N. Kidonakis, Phys.Rev. D81 (2010) 054028, 1001.5034.

[61] N. Kidonakis, Phys.Rev. D82 (2010) 114030, 1009.4935.

[62] M. Czakon, A. Mitov and G.F. Sterman, Phys.Rev. D80 (2009) 074017, 0907.1790.

[63] M. Neubert, Phys.Rept. 245 (1994) 259, hep-ph/9306320.

[64] C. W. Bauer, S. Fleming, D. Pirjol, I. W. Stewart,
Phys.Rev. D63 (2001) 114020, hep-ph/0011336.

[65] C.W. Bauer, D. Pirjol and I.W. Stewart, Phys.Rev. D65 (2002) 054022, hep-ph/0109045.

[66] M. Beneke, A.P. Chapovsky, M. Diehl and T. Feldmann,
Nucl.Phys. B643 (2002) 431, hep-ph/0206152.

[67] V. Ahrens, A. Ferroglia, M. Neubert, B.D. Pecjak and L.-L. Yang,
Phys.Lett. B687 (2010) 331, 0912.3375.

[68] V. Ahrens, A. Ferroglia, M. Neubert, B.D. Pecjak and L.-L. Yang,
JHEP 1009 (2010) 097, 1003.5827.

[69] V. Ahrens, A. Ferroglia, M. Neubert, B.D. Pecjak and L.-L. Yang,
JHEP 1109 (2011) 070, 1103.0550.

[70] V. Ahrens, A. Ferroglia, M. Neubert, B.D. Pecjak and L.-L. Yang,
Phys.Lett. B703 (2011) 135, 1105.5824.

[71] A. Ferroglia, B.D. Pecjak and L.-L. Yang, JHEP 1210 (2012) 180, 1207.4798.

[72] A. Ferroglia, B.D. Pecjak and L.-L. Yang, Phys.Rev. D86 (2012) 034010, 1205.3662.

[73] A. Ferroglia, S. Marzani, B.D. Pecjak and L.-L. Yang, JHEP 1401 (2014) 028, 1310.3836.

[74] N. Kidonakis and B.D. Pecjak, Eur.Phys.J. C72 (2012) 2084, 1108.6063.

[75] N. Kidonakis and G.F. Sterman, Phys.Lett. B387 (1996) 867.

[76] N. Kidonakis, (2013), 1311.0283.

[77] T. Becher and M. Neubert, Phys.Rev. D79 (2009) 125004, 0904.1021.

[78] N. Kidonakis, Phys.Rev.Lett. 102 (2009) 232003, 0903.2561.

[79] A. Mitov, G.F. Sterman and I. Sung, Phys.Rev. D79 (2009) 094015, 0903.3241.

[80] A. Mitov, G.F. Sterman and I. Sung, Phys.Rev. D82 (2010) 034020, 1005.4646.

[81] M. Czakon and P. Fiedler, Nucl.Phys. B879 (2014) 236, 1311.2541.

[82] P.M. Nadolsky, H.-L. Lai, Q.-H. Cao, J. Huston, J. Pumplin, D. Stump, W.-K. Tung, C.-P. Yuan, Phys.Rev. D78 (2008) 013004, 0802.0007.

[83] A.D. Martin, W.J. Stirling, R.S. Thorne and G. Watt, Eur.Phys.J. C63 (2009) 189, 0901.0002.

[84] J. Gao, M. Guzzi, J. Huston, H.-L. Lai, Z. Li, P.M. Nadolsky, J. Pumplin, D. Stump and C.-P. Yuan, Phys.Rev. D89 (2014) 033009, 1302.6246.

[85] S. Alekhin, J. Blümlein and S. Moch, Phys.Rev. D86 (2012) 054009, 1202.2281.

[86] ZEUS Collaboration, H1 Collaboration, A. Cooper-Sarkar, PoS EPS-HEP2011 (2011) 320, 1112.2107.

[87] NNPDF Collaboration, R.D. Ball, V.Bertone, S.Carrazza, C.S. Deans, L. Del Debbio, S. Forte, A. Guffanti, N.P. Hartland, J.I. Latorre, J. Rojo and M. Ubiali,
Nucl.Phys. B867 (2013) 244, 1207.1303.

[88] Particle Data Group, J. Beringer et al., Phys.Rev. D86 (2012) 010001.

[89] M. Dowling and S. Moch, (2013), 1305.6422.

[90] S. Alekhin, J. Blümlein and S. Moch, Phys.Rev. D89 (2014) 054028, 1310.3059.